Role of structural defects in the adsorption and separation of C3 hydrocarbons in Zr-fumarate-MOF (MOF-801)

Paul Iacomi [†, a], Filip Formalik [†, b, c], João Marreiros [d], Jin Shang [e], Justyna Rogacka [b], Alexander Mohmeyer [f], Peter Behrens [f], Rob Ameloot [d], Bogdan Kuchta [a, b], and Philip L. Llewellyn [*, a]

[a] Aix-Marseille University, CNRS, MADIREL (UMR 7246), 13013 Marseille, France
[b] Bioprocess and Biomedical Engineering Group, Faculty of Chemistry, Wroclaw University of Science and Technology, Wybrzeże Wyspiańskiego 27, 50–370, Wrocław, Poland
[c] Department of Theoretical Physics, Faculty of Fundamental Problems of Technology, Wroclaw University of Science and Technology, Wybrzeże Wyspiańskiego 27, 50–370, Wrocław, Poland
[d] Centre for Surface Chemistry and Catalysis, KU Leuven, Celestijnenlaan 200F, P.O. Box 2461, 3001 Leuven, Belgium
[e] School of Energy and Environment, City University of Hong Kong, Tat Chee Avenue, Kowloon, Hong Kong SAR, People's Republic of China
[f] Institute for Inorganic Chemistry, Leibniz Universität Hannover, Callinstr. 9, 30167 Hannover, Germany.

† these authors contributed equally
* *philip.llewellyn@univ-amu.fr*

An effective separation of propylene/propane mixtures is one of the most important processes in the petrochemical industry. Incidentally this separation is challenging due to the extensive similarities between both gases in terms of physicochemical properties such as, but not only limited to, boiling point, kinetic diameter and molecular weight. A drive to switch to energy efficient processes, like adsorption or membrane separation, has highlighted several microporous metal organic frameworks as promising materials. In this work, we present a combined numerical and experimental investigation on propane and propylene adsorption in Zr-fumarate-MOF (also known as MOF-801), a small pore isoreticular analogue of UiO-66. Here, we demonstrate how the presence of structural defects can completely change the sorptive properties and separation performance of the Zr-fumarate-MOF, with the loss of sieving effects and a reversal of selectivity towards propane, as well as enhanced capacity and diffusion rates for C3-sized hydrocarbons. Extensive GCMC simulations performed on mixed defective supercells show that a ratio of missing cluster defects of around 1/8th can best account for the experimental results. Furthermore, analysis of low-frequency phonon spectra is used to explain gaseous diffusion in the original pristine material. Finally, the thermodynamic preference for propane over propylene is confirmed through column breakthrough experiments, suggesting the potential applicability of the Zr-fumarate-MOF in this challenging separation.

Keywords: metal-organic frameworks; gas adsorption; paraffin-olefin separation; defect engineering

1. Introduction

One of the most challenging large-scale separations is that of propane/propylene mixtures, a common by-product in conventional olefin or fluid catalytic cracking plants, or as the main output of targeted propylene synthesis, such as propane dehydrogenation. With the abundance of natural propane from shale gas in recent years, and the increasing global demand for propylene the latter is becoming more industrially attractive [1]. The current standard practice for this separation is cryogenic distillation, an energetically intensive process, requiring compression of the gas mixture and low temperatures [2]. Furthermore, owing to the similar physical properties of propane and propylene (boiling points, vapour pressure, etc.), commonly employed distillation columns require a large number of stages and reflux ratios, increasing the overall energy cost. Consequently, the development of alternative separation avenues is crucial for reducing the production cost of this industry relevant olefin.

A promising alternative can be found in the use of porous materials to perform the separation through adsorptive means, either based on the thermodynamics or kinetics of physisorption, or otherwise through molecular sieving [3]. The shift to such methods is particularly attractive due to the relatively low energy cost of adsorbed phase recovery when compared to current practices [4]. Performance of said processes greatly depends on the properties of the adsorbent materials, as well as the capability for proper and controlled structuring of these sorbents into beads, columns or membranes. To date, considerable studies have been reported on the matter, with particular focus on the use of polymers [5–7], carbonaceous materials [8–10], or zeolites [3,11–16] as the porous media.

Thermodynamic separation is achieved through equilibrium concentration differences in the adsorbed phase, caused by a difference in the strength of attractive interactions between components in the mixture and the adsorbent surface. Propylene selectivity in such a process is usually due to interactions involving the π electrons of the double bond [17,18]. Instead, when specific guest-host interactions are absent, a slight propane selectivity can be observed [8,19], attributed to larger intermolecular interactions of the saturated molecule [10]. Kinetic separations rely on differences in gaseous diffusion rates in a pore network, and are necessarily transient or flow-based processes, used in columns or membranes. Diffusion can be dominated either by size-controlled diffusion, where the smaller component is generally selected for retention, or surface diffusion after adsorption, in which the stronger adsorbed component is preferably retained [20]. The kinetic diameter difference between propylene (0.40 nm) and propane (0.43 nm) [21] is minimal, requiring a material with a well-defined

Electronic Supplementary Information (ESI) available: one PDF file with all referenced supporting information and CIF files corresponding to pristine and defective structures investigated.

pore entrance and very narrow pore size distribution if kinetic separation is desired. Such a process can be encountered in small window DDR zeolites[22–24] where faster propylene diffusion leads to its preferential adsorption. Finally, molecular sieving occurs when the pore apertures in the adsorbent material are simply too small for one mixture component to enter the pore.

Metal-organic frameworks (MOFs) have been an intensely studied area in materials science, owing to their potential as highly tunable materials. Indeed, with judicious design, the skilled chemist can manipulate pore shape, window size, surface interactions and even introduce stimuli-responsive material changes through decoration of a particular topological net. These materials offer promise in areas of gas adsorption such as storage and separation, where conventional adsorbents fail to achieve the desired performance, and where their unique characteristics (tunability, defects, compliance, etc.) can be leveraged for highly specific applications. In the area of propane/propylene separations, MOFs have been the focus of several avenues of study. Frameworks with open metal sites, such as copper paddlewheels[25,26], iron trimers[27] or the closely-related family of hexacyanometallates[28] have been shown to preferentially adsorb propylene due to specific interactions with these sites. Alternatively, the isoreticular chemistry approach can be employed to obtain pore window sizes in the exact range required for kinetic separation[29], or molecular sieving[30]. Furthermore, MOF zeolite analogues such as ZIF-8[31,32] and ZIF-7[33,34], have shown promise for parrafin/olefin separations, due to the disparity in diffusivities introduced by the small cage entrances and gate opening effects[35].

Zr-fumarate-MOF[36], later renamed to MOF-801[37], is a fumaric acid analogue of the topical UiO-66(Zr) framework. It shares the same face-centered cubic (**fcc**) topology, with inorganic clusters interconnected by a smaller, non-linear dicarboxylate linker, leading to a lowering of symmetry and slight tilting of the $[Zr_6(\mu_3\text{-}O)_4(\mu_3\text{-}OH)_4]^{12+}$ clusters, as depicted in Fig. 1. Synthesis can only take place under modulation/coordination conditions, using considerable amounts of competing monotopic acids as the modulator, resulting in higher crystallinity and yield of the material. Indeed, when not using this approach, the resulting material is nearly amorphous[38]. Zr-fumarate-MOF has recently been the subject of scientific interest due to its high water stability[39], as well as its potential for green synthesis[40] and facile shaping through direct monolith formation by a gel approach[41]. The material has a remarkably steep water adsorption isotherm at low relative pressure[37], which led to its possible application as a water scavenger membrane[42], or in a water harvesting device which would capture water from air in low relative humidity environments[43]. This low pressure condensation step for water has highlighted the contribution of defects in shifting the adsorption isotherm, an effect arising from cooperative interactions and initial clustering of water molecules at defect sites[44]. The window diameter of the Zr-fumarate-MOF is in the same length scale as C3 hydrocarbons, an aperture size which has been shown in studies on similar **fcu** MOFs[30] to be suitable for kinetic or exclusion-driven separations. For these reasons, this MOF was previously highlighted as prime candidate for propane/propylene separations[45]. However, the presence of structural defects may have a large impact on the adsorption of these gases.

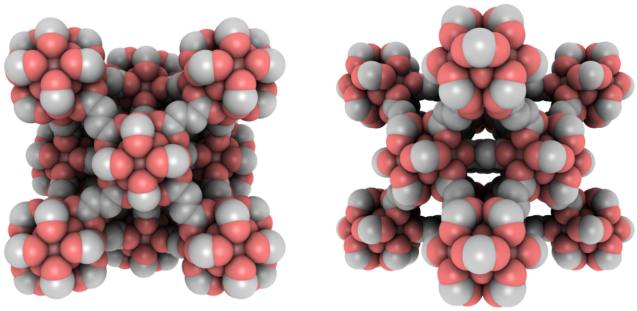

Fig. 1. Structure of Zr-*fum*-MOF: front (left) and side (right) views (generated by iRASPA software[46])

In the following we present a combined computational and experimental approach describing the adsorption behaviour of saturated and monounsaturated C3 hydrocarbons in a defect-rich Zr-*fum*-MOF system. We evaluate the contribution of defects in the synthesised material and demonstrate their crucial impact on the diffusion of the gaseous phase in the crystalline MOF. Grand Canonical Monte Carlo (GCMC) adsorption simulations are performed on several structural models containing a range of defects, of varying nature and concentration/distribution, to reproduce experimental isotherms. We also perform calculations of phonon spectra, revealing the potential for pore window deformations, which can explain previously observed diffusion of gases in the pristine version of the material[45]. The enthalpies of adsorption of propane and propylene are both calculated through the Widom insertion method and measured *in situ* through microcalorimetry, with propane adsorption shown to be more energetically favourable. This can be correlated with a higher selectivity for propane over propylene in mixture co-adsorption experiments, predicted through Ideal Adsorbed Solution Theory (IAST) and *in silico* simulations, and further investigated by column breakthrough experiments. As opposed to a perfect material, defects are shown to drastically increase the uptake of all probes and to increase the mobility probability through the newly generated voids (missing structural elements = more free space = less physical/steric impediment). We then discuss the unexpected thermodynamic selectivity in the defective material which runs opposite to the sieving effect which has been observed in a pristine structure[45].

2. Results and discussion

2.1. Sample synthesis and preliminary characterisation. The Zr-fumarate-MOF sample was synthesised following the previously reported method[47], where a large excess of formic acid (100 equivalents) is added together with the MOF precursors in water as the reaction medium, to obtain a white precipitate of Zr-*fum*-MOF crystals. For further characterization the precipitate was Soxhlet-extracted with ethanol and afterwards dried under reduced pressure. Phase purity of the resulting powder was confirmed by comparing experimental powder X-ray diffraction (PXRD) patterns to those simulated from structural data (Fig. S2). Scanning electron microscopy (SEM) of the MOF revealed well-defined octahedral crystals with an average diameter of 100–200 nm (Fig. S1).

Nitrogen physisorption recorded at 77 K was used to determine a Brunauer-Emmet-Teller (BET) specific surface area

of 963 m^2/g and a t-plot calculated micropore volume of 0.38 cm^3/g. The pore size distribution calculated from this isotherm shows two peaks, corresponding to the tetrahedral and octahedral cages, respectively (Fig. S5). However, the distribution also indicates that pores larger than the crystal structure would suggest (in the 1–2 nm range) are present, accounting for a substantial increase in volumetric uptake and strongly supporting the existence of structural defects. The thermogravimetric curve (Fig. S3) recorded in an air atmosphere shows a pronounced mass loss below 400 K, as the large amount of water and other guests in the structure are removed. Two further steps are observed: one at 600 K, corresponding to the degradation and subsequent oxidation of the organic linker, with a further step around 830 K which has been previously associated to the decomposition of zirconium-coordinated carbonate groups[36,39]. We further confirm the similarity of the synthesised material with existing literature by recording water adsorption at 298 K. The resulting isotherm (Fig. S6) shows a pronounced pore condensation step at $\approx 0.1\ p/p^0$ and near-complete reversibility in the desorption branch, in accordance with previous results[37,44].

2.2. Adsorption microcalorimetry screening. To screen the Zr-fumarate-MOF for potentially interesting adsorption properties, the isotherms of 9 probe gases (Ar, N_2, O_2, CO, CH_4, CO_2, C_2H_6, C_3H_8, C_3H_6) were recorded in a microcalorimeter, allowing for a measurement of the differential enthalpy of adsorption ($\Delta_{ads}h$) for each isotherm point. The entire dataset is available in Fig. S8. The material shows relatively flat, gently decreasing enthalpy curves for Ar, N_2, O_2, CO and CH_4, corresponding to adsorption on homogenous sites. In contrast, enthalpy curves for CO_2, C_2H_6, C_3H_8 and C_3H_6 show a sharp decrease in $\Delta_{ads}h$, to a lower plateau, suggesting an initial preferential interaction followed by weaker interactions with the pore surface. These four probes are the only ones for which the isotherm plateau is reached in the pressure range studied, corresponding to complete pore filling. More interestingly, the enthalpy of adsorption of propane in the low-loading region (<2 mmol g^{-1}) is found to be higher on average than that of propylene. If the enthalpy curve is extrapolated to obtain the enthalpy of adsorption at zero loading ($\Delta_{ads}h_0$), values of $\approx$38 kJ mol^{-1} and $\approx$44 kJ mol^{-1} are obtained for propylene and propane, respectively, suggesting a stronger guest-host interaction with the saturated molecule. This result is unexpected, as propylene is commonly thermodynamically preferentially adsorbed in most previously studied adsorbent materials, owing to increased interactions between the double bond and framework features such as open metal sites. In order to put this difference into perspective $\Delta_{ads}h_0$ has been calculated for the entire series of probes, together with the initial Henry constant ($H_{K,0}$), another measure of structure-adsorbate interactions, and plotted versus the specific polarizability of each probe molecule (Fig. 2). Probes which interact with the framework through non-specific interactions, such as noble gases and unsaturated hydrocarbons, are expected to exhibit a linear evolution of $\Delta_{ads}h_0$ and $H_{K,0}$ with respect to their polarizability. In such a case, the slope of the resulting correlation line is representative of the field gradient encountered in the pore where adsorption takes place. We can observe that both values for propylene fall below the predicted linear relationship. It could be argued that the slow uptake kinetics of the gas at low loading may influence the recorded heat flow. However, when observing the time-resolved uptake for the 0–0.05 bar pressure range (Fig. S9), the adsorption kinetics for both gases do not differ significantly on this material.

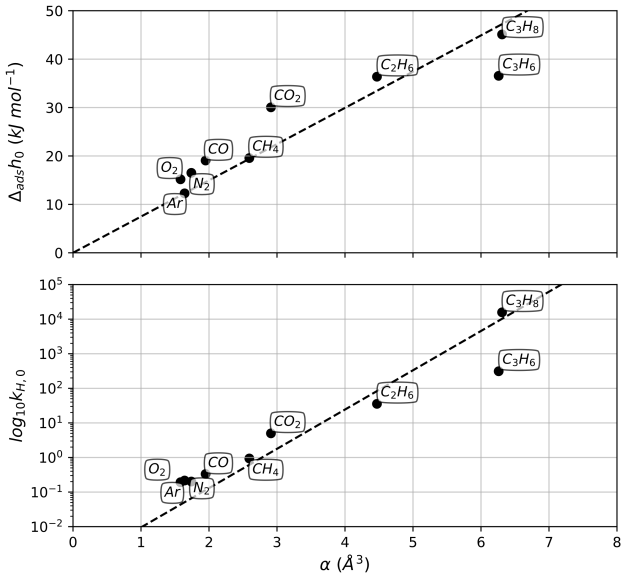

Fig. 2. Zero-loading differential enthalpy of adsorption (top) and logarithm of initial henry constant (bottom) plotted against the polarizability of each specific gas molecule. Dotted lines are least square fits to the y axis values for C1-C3 saturated hydrocarbons.

2.3. C3 adsorption in pristine Zr-fumarate-MOF. To focus on the unusual C3 hydrocarbon measurements, propane and propylene single component adsorption isotherms were recorded separately (Fig. 3). The isotherms show a larger amount of propylene adsorbed at saturation, as expected due to the higher packing efficiency of propylene and its consequently higher fluid phase density. However, a cross-over is observed around 0.1 bar, with propane capacities overtaking its unsaturated analogue below this pressure. To understand the microscopic mechanism of the single component adsorption of propane and propylene, we turn to *in silico* methods. Using Monte Carlo simulations within the grand canonical ensemble (GCMC methods) we can simulate gas adsorption and model isotherms in a MOF structure, real or hypothetical.

The adsorption isotherms obtained for the ideal (non-defective) structure significantly differ from the experimental results (overlaid in Fig. 3). The uptake calculated in the low-pressure region exceeds the experimental values, which can be attributed either to (i) inaccuracies in the force field definition, especially of the ε value, responsible for the strength of the interactions between molecules, as well as host-guest interactions (through Lorentz-Berthelot mixing rules) or to (ii) the existence of stronger adsorption sites which do not exist in the experimental sample. On the other hand, modelled results underestimate uptake for higher pressures (>0.1 bar) where the experimental uptake substantially exceeds the theoretical values by almost 75%. As before, the divergence can be attributed to the definition of the size of the molecules in the force field (σ parameter) or further interpreted as the existence of pores of different diameters in ideal and real structures. In this study

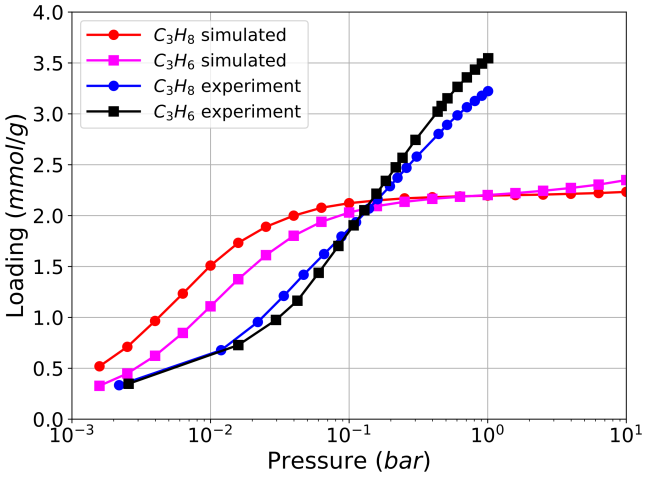

Fig. 3. Experimentally measured isotherms on the Zr-fumarate-MOF sample (blue and black) compared to simulated adsorption in the ideal structure of Zr-fumarate-MOF (red and pink) of propane (round markers) and propylene. Isotherm confidence ranges are below 2% and are not shown on the graph.

we made use of the force field developed by the group of Sofia Calero[48] to accurately describe vapour-liquid curves for alkanes and alkenes. As it has been successively tested in GCMC simulations of adsorption of hydrocarbons for wide range of zeolites and MOFs[49–52], we do not anticipate our choice of force field to be the source of significant differences between calculated and measured uptakes. We therefore attribute such differences to the non-realistic, ideal structure of the Zr-fumarate-MOF used in the first set of GCMC calculations. However, the simulated isotherms qualitatively agree with the measured ones (preference of propane in lower pressures and propylene in higher). We can relate it to two properties of the analysed molecules — (i) heat of adsorption of propane ($42.7\,\mathrm{kJ\,mol^{-1}}$ with GCMC and $44\,\mathrm{kJ\,mol^{-1}}$ in calorimetry) is slightly higher than for propylene ($39.7\,\mathrm{kJ\,mol^{-1}}$ with GCMC and $38\,\mathrm{kJ\,mol^{-1}}$ in calorimetry) which promotes the initial uptake of alkane and (ii) aforementioned diameters of molecules (0.43 nm for propane and 0.4 nm for propylene) — smaller molecules are simply packed in the pore with higher density.

To examine the distribution of molecules in the material pores we calculated density maps. Fig. 4a presents two cross-sections of such maps, for propane and propylene. It can be seen that there are areas with finite values of density surrounded by the large areas (blue on Fig. 4a) where adsorbate density is zero, or inaccessible regions for insertion. Several regions exist where the pockets of density are thinly (or nearly) connected, corresponding to the pore windows. These results indicate that diffusion between the gates in the perfect structure is unlikely to occur, which is contradictory to what has been measured experimentally[45]. One possible explanation for the hydrocarbon uptake can be the presence of a vibrationally-induced gate opening effect, as has been observed in MOFs such as ZIF-4, ZIF-7 and ZIF-8[53]. To check how the flexibility of the framework affects the sizes of the gates, phonon calculations were performed (details of the methodology can be found in the SI). For our analysis we selected modes of low frequency ($<130\,\mathrm{cm^{-1}}$) since, as previously suggested, they may reflect potential adsorption-induced deformations of the framework[53,54]. We distinguished two separate collections of modes: 0–83 $\mathrm{cm^{-1}}$ and 92–129 $\mathrm{cm^{-1}}$, which correspond to rotation and translation of the metallic cluster and vibrations of the fumarate linkers, respectively. To ascertain whether some of those modes can be related to enlargement of the gate connecting two neighbouring cages we have generated structural snapshots of the material according to the deformation indicated by a particular mode with an arbitrary amplitude (positive and negative, CIF files available as SI). We then calculated the pore limiting diameter (PLD) using Poreblazer[55] and selected the modes which increase this value (see Fig. S13). For ten modes which show the largest increase of the PLD we calculated density maps, to check if the proposed deformations can connect the cages within the material. Resulting isosurfaces are presented in Fig. S14. In particular, the mode located at $115.1\,\mathrm{cm^{-1}}$, which can be described by a trampoline-like motion of the linkers (Fig. 4b), appears to be a good candidate for a gate-enlargement process. Calculated density distributions (Fig. 4c) show that diffusion in the material deformed according to this particular phonon is possible and can explain the experimentally-observed results of Liu *et al.*[45].

While vibrational modes can favour adsorbate diffusion in the pristine material, they do not shed light on the differences in adsorption kinetics, or the larger capacity than theoretically predicted. We must therefore examine the possibility of structural defect contribution. Indeed, a density map calculated for a unit cell with a missing cluster (Fig. 4d) shows unobstructed communication between structural voids and may hold clues as to why the material used in this study readily adsorbs both probes. An in-depth look at the contribution of defects takes place in the next section.

2.4. Evidence for defects. A peculiar characteristic of the Zr-fumarate-MOF is that, as reported in the original synthesis methodology, no crystalline material can be formed without the addition of a modulator, with excess formic acid improving the crystallinity of the obtained powder. This approach is well known to promote defect generation in the UiO-66 framework, with higher amounts of modulator leading to increased defect concentration[56], and can be expected to extend to its isoreticular analogues. It has been previously shown that structural defects can drastically alter adsorption behaviour and are commonly found in the high connectivity networks of multi-coordinated zirconium cluster MOFs[57–59]. Indeed, experiments investigating the Zr-fumarate-MOF for the separation of butane isomers[60] have found that iso-butane uptake becomes non-negligible when the MOF is synthesised with a large modulator excess. As iso-butane molecules are too large to pass through the cage windows, the presence of additional porosity or cage widening can explain such results.

It is therefore reasonable to assume that the presence of structural defects in the Zr-fumarate-MOF may account for the observed discrepancy between experimental and modelled isotherms. The decreasing enthalpy profiles equally suggest some form of energetic heterogeneity. Choi and co-workers[44] have interpreted the low relative pressure at which water condenses in the small pores as a guest collaborative effect resulting from the presence of missing linker defects. With this in mind, five model structures were designed in identical configurations as reported by Choi *et. al.*, herein referred to as ml_1, ml_2_90, ml_2_180, ml_2_par and ml_4 (CIF files available as SI). The prefix stands for *missing linker*, followed by the number and, where applicable, the relative positions

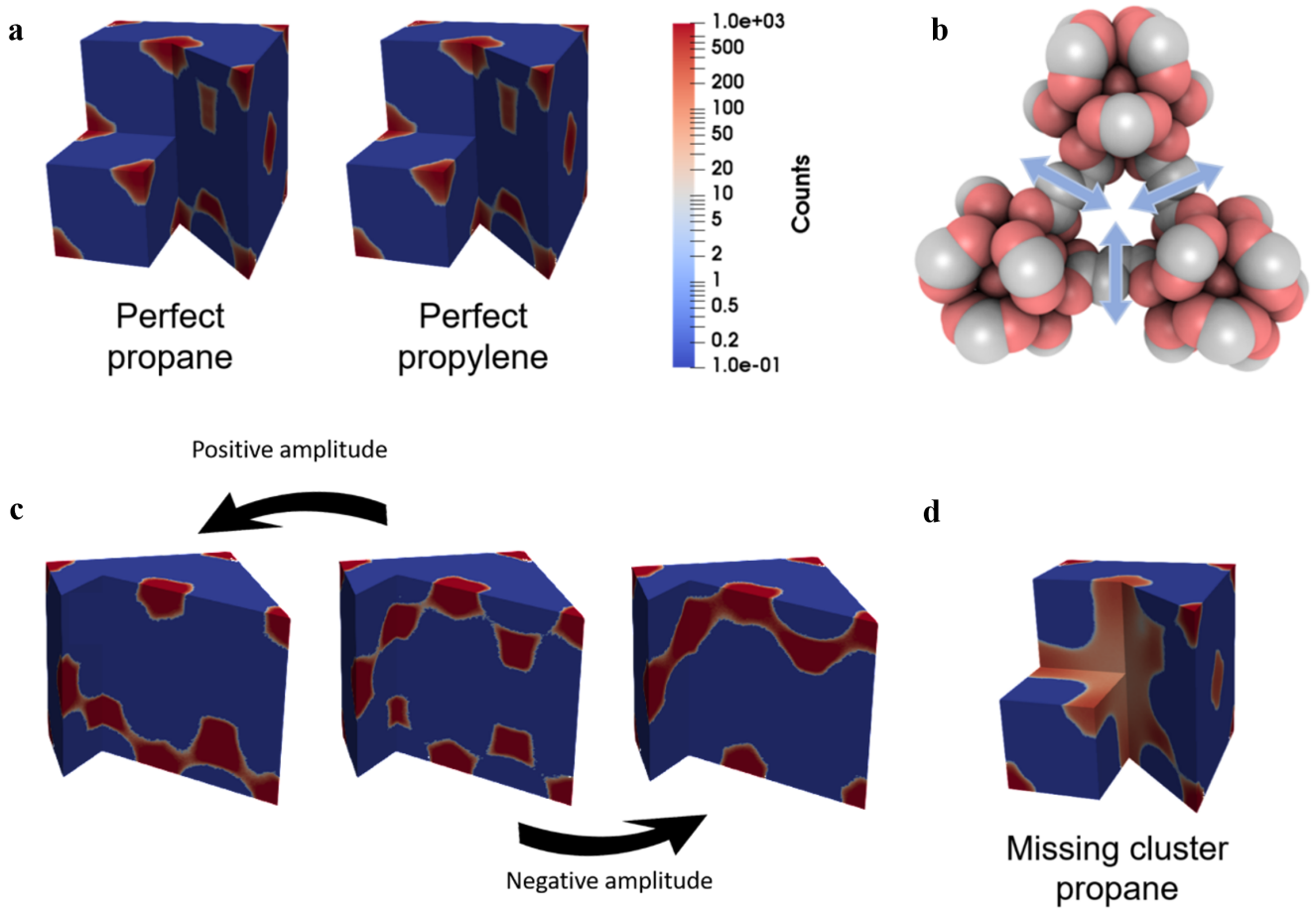

Fig. 4. (a) Density maps for propane and propylene adsorption in an ideal structure of Zr-fumarate-MOF. The propylene density map (right) is seen to be nearly identical to propane (left). A logarithmic scale is used for density visualization. (b) Trampoline-like mode related to gate-enlargement. (c) Density maps for structure deformed according to the trampoline-like phonon. (d) Density map for adsorption in a missing cluster.

where linkers were removed (see Fig. 5a). For charge compensation, missing linkers were substituted by two formic acid capping molecules, as this is the modulator available during synthesis and it is expected to remain coordinated to the metal sites[58]. Fig. 5 shows the simulated adsorption isotherms of propane (b) and propylene (c) for the missing linker structures. Regardless of their distribution, the introduction of missing-linker defects did not change the characteristics of the simulated isotherms, leading only to a slight increase in uptake for pressures approaching 10 bar. Due to the small size of the fumarate linker compared to other isoreticular analogues, its removal and subsequent formate capping does not generate a significantly larger void space in the structure.

Alternative types of structural imperfections include missing-cluster-type defects. It has been reported that this type of structural deviation from the ideal structure leads to decreased adsorption in the low-pressure region, followed by an increase in the uptake at higher-pressures[61] and may explain the experimental results. In order to test this hypothesis, a new framework model was constructed, considering a missing-cluster defect. Assembly of the new model consisted in the removal of an entire inorganic cluster, together with the connecting linkers and subsequent capping of open metal sites in adjoining clusters with formate ions. We artificially introduced several such configurations in a $2 \times 2 \times 2$ supercell, with no adjoining defects — with $1/4^{\text{th}}$, $3/16^{\text{th}}$, $1/8^{\text{th}}$ and $1/16^{\text{th}}$ of the total number of clusters removed (as shown in Fig. 5d) and further referred to as mc_1_4, mc_3_16, mc_1_8, mc_1_16 (mc — *missing cluster*). The resulting CIF files are available as Supplemental Information. Fig. 5e-f shows the calculated isotherms for the aforementioned structures and confirms that the absence of metallic clusters in the structure of the Zr-fumarate-MOF is responsible for the observed shift of the pore-filling step and higher total capacity in the experimental results. In addition, quantitative conclusions can be drawn — we see that the isotherm predicted by mc_1_8 ($1/8^{\text{th}}$ missing total clusters) is the best fit to the measured isotherm — practically a full overlap for propane and a slight underestimate for propylene at higher pressures. It is worth highlighting that these isotherms are calculated in a periodic supercell, introducing artificial long-range periodicity of defects, possibly unrepresentative of the real sample. The results are interpreted in a statistical manner such that a structure with a particular concentration of defects can be a possible candidate to describe experimentally observed adsorption.

Physical evidence for structural defects may be obtained from characterisation techniques such as TGA, ^{1}H NMR and high resolution XRD. The thermogravimetric curve can be used to gauge the percentage of missing linker defects in the

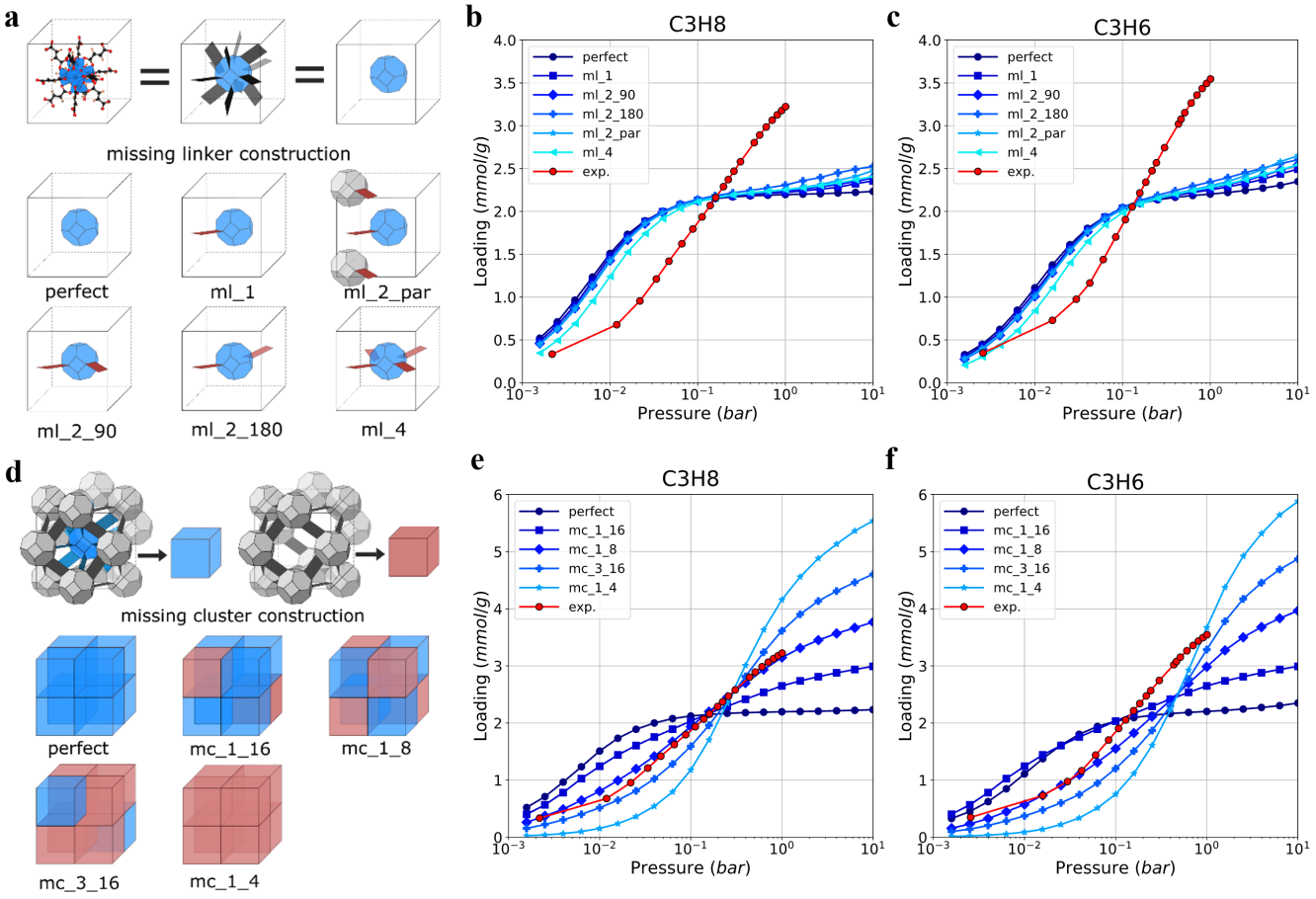

Fig. 5. Depiction of assessed defect types (a) missing linker type defects and (d) missing cluster type defects and corresponding supercells. Uptake of propane in Zr-fumarate-MOF with missing linker-type defects (b) and with missing cluster-type defects (e). Uptake of propylene in Zr-fumarate-MOF with missing linker-type defects (c) and with missing cluster-type defects (f).

structure (as has been previously reported[62]) by stoichiometrically calculating the weight ratio at 550 K (where it is assumed that any adsorbed water, residual solvent and defect site cappers have been removed) to the inorganic residue after combustion in the oxygen-rich atmosphere at 937 K (corresponding to ZrO_2). The resulting cluster-to-linker ratio for the Zr-fumarate-MOF sample is found to be around 5. This organic to inorganic balance, below the ideal value 6 for the defect-free MOF, confirms the presence of structural defects in the experimental sample. Unfortunately, the thermogravimetric method cannot differentiate between missing linker- and missing cluster-type defects. If assuming only missing cluster-type defects are present, their concentration can be calculated as 1/7, remarkably close to the simulated best-fitting ratio of 1/8.

To further shed light on the nature of the underlined structural defects, solution ^{1}H NMR was performed on a NaOD digested sample. The resulting spectrum (Fig. 6) reveals the presence of 3 distinct and well resolved singlet peaks attributed to water (4.79 ppm), fumarate (6.23 ppm), and formate (8.17 ppm). The observed water signal demonstrates its presence in the structure and can be attributed to several sources: (i) an adsorbed phase in the pores or (ii) defect sites which are capped by water molecules or hydroxide groups instead of formate groups. This structural H_2O can be traced either to the initial synthesis, or through latter adsorption due to the high Zr-fumarate-MOF affinity for atmospheric water. As water capping is energetically favoured[63] but cannot be deconvoluted from the adsorbed phase, we will only consider the ratio of carboxylates, with the mention that more defect sites than calculated are likely to exist in the sample. Based on the normalized integrated areas of the fumarate and formate signals and under the assumption that these are the only structural elements of the framework, we determine that the components are present in a proportion of 15:1 for fumarate and formate, respectively. Given this ratio and further considering missing cluster defects as the only type present, we estimate that for every 3 perfect unit cells a fourth unit cell with a missing cluster defect exists, or 1/16 missing clusters. This ratio, lower than that determined through TGA or GCMC, points to the existence of water capped defect sites alongside formate.

Neither TGA nor ^{1}H NMR can differentiate between missing linker and missing cluster defects, so no prediction of selective preponderance in the structure can be made. However, if the predicted missing cluster defects are present in a correlated fashion, clues may arise in the PXRD pattern. The **reo** phase has been demonstrated to cluster defects in correlated nanodomains during synthesis for the sibling UiO-66 when prepared in formic acid rich conditions, giving rise to symmetry forbidden signals in the low 2θ range[62,64–66].

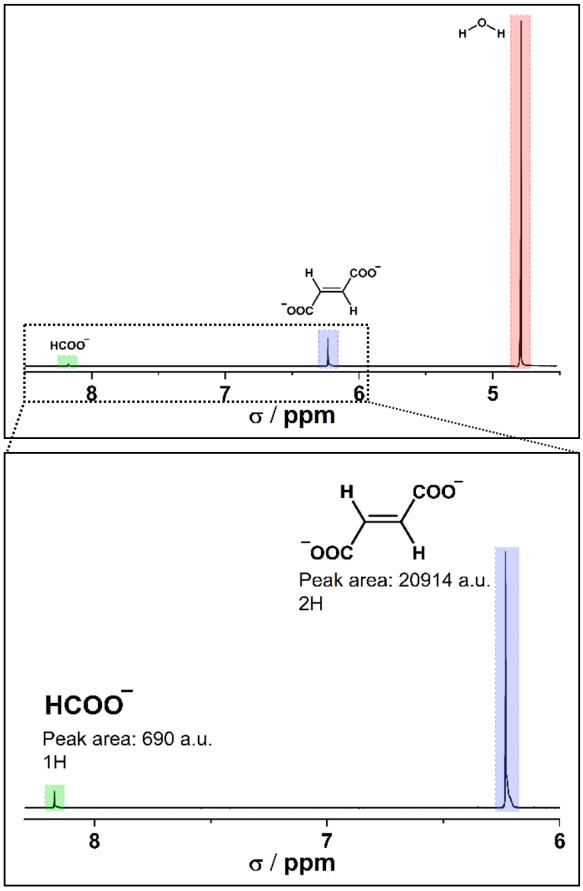

Fig. 6. ^{1}H NMR of Zr-fumarate-MOF with highlighted 9–6 region and integrated peaks for formate and fumarate in green and blue, respectively. The peak corresponding to water is displayed in red.

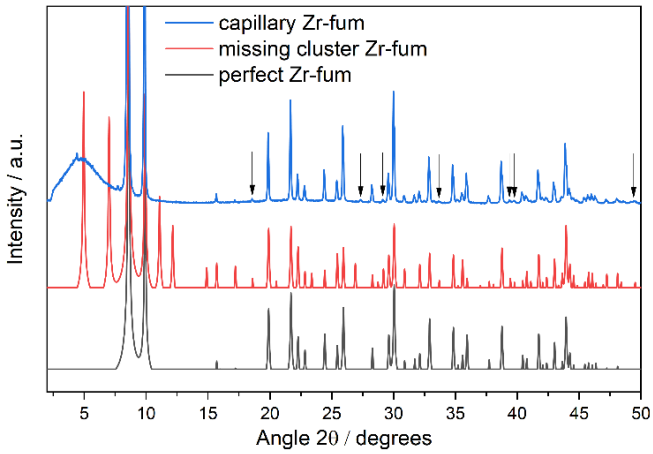

Fig. 7. Capilary XRD of Zr-fumarate-MOF sample (blue) with simulated patterns of the fcu (black) and reo (red) phases.

The presence of these reflections can therefore be employed as a benchmark for the occurrence of the secondary phase with lower cluster content. Indeed, a second high-resolution capillary XRD characterization of the activated framework reveals the characteristic profile of Zr-fumarate-MOF (blue in Fig. 7) accompanied by low intensity signals, supporting the existence of missing cluster defects in conformity with previous reports on isoreticular Zr MOFs. The experimental pattern did not display the typical **reo** phase (100) and (110) plane reflections but a broad diffuse scattering signal in the low angle region (2.3°-7.6°) leading us to hypothesize the presence of low amount of highly dispersed missing clusters arranged in non-correlated fashion. Careful examination of the sample's diffractogram reveals the presence of well-defined, low intensity reflections indexed exclusively to the missing cluster structure (black arrows in Fig. 7) for 2θ angles greater than 16 degrees, suggesting the presence of missing cluster defects with short range ordering or correlation. We can therefore conclude, with a high degree of certainty, that the sample in question does in fact carry missing cluster defects responsible for the formation of a distinct defective **reo** phase. However, it is present in minor abundance compared to the regular **fcu** phase.

A parallel can be made with the smallest currently known analogue of the UiO-66 isoreticular series, zirconium squarate (ZrSQU) synthesised by Bueken *et al.*[67]. In ZrSQU, the crystal structure predicts no possible adsorption of even smaller molecules, such as nitrogen. The presence of what the authors suggest to be missing linker defects leads to an accessible porosity in N_2 physisorption (although no computational study of the diffusion of nitrogen into the proposed defective structure was made). It is however likely that, in a system which is even more confined than the Zr-fumarate-MOF, a larger preponderance of missing cluster defects can be present, as suggested by the broad reflections at low angles of the PXRD pattern in the original publication indicative of a mixed phase framework with coexistence of **fcu** and **reo** forms.

2.5. Separation of propane-propylene mixtures. To evaluate the material for thermodynamic propane-propylene separation, simulations of equimolar mixture adsorption were performed in previously-mentioned structures. The simulated selectivity (α) of the ideal structure, ml_1, ml_4, mc_1_8 and mc_1_4 is shown in Fig. 8a, while the rest can be found in the Supplemental Information (Fig. S15). It should be noted that the values in Fig. 8a are obtained with the assumption of equilibrium and complete adsorbate access to the entire porous network. It is to be expected that in the pristine structure, apparent selectivity would be dependent on diffusion and size exclusion. Selectivity can be seen to be above unity for propane, and decrease with higher total mixture pressure, even with the presence of defects. Starting from pure component isotherms, ideal adsorbed solution theory (IAST) can also forecast multi-component adsorption selectivity at different pressures. The calculated selectivity curve, shown in Fig. S10, predicts a slightly lower selectivity than what is obtained through co-adsorption simulations with a α of around 1.3 for propane at 0.2 bar total pressure, also decreasing with higher pressures.

As previously mentioned, both simulated co-adsorption and IAST predictions assume thermodynamic equilibrium between the gaseous and adsorbed phases. No difference in equilibrium time was observed in pure component adsorption (Fig. S9). To further evaluate the impact of possible kinetic or size exclusion effects, breakthrough adsorption experiments were carried out with a C_3H_6:C_3H_6:Ar = 5:5:90 gas mixture at 295 K and 1 bar/5 bar total pressure. Argon was chosen as the carrier gas due to its inert nature and negligible uptake when compared to the hydrocarbons. The breakthrough curves recorded at 1 bar (Fig. 8b) show the material indeed adsorbs propane over

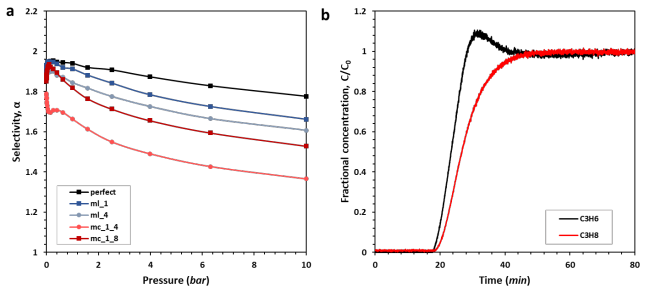

Fig. 8. (a) Simulated selectivity of a 1:1 molar mixture of propane and propylene at various total mixture pressure. Black, blue and red represent pristine, missing linker and missing cluster structures, respectively. (b) Breakthrough curves of an equimolar propane-propylene mixture in carrier gas at a total inlet pressure of 1 bar. Propane is in red and propylene in black.

propene, and that the selectivity (as calculated through Eq. S2) is 1.28, remarkably consistent with the IAST prediction. At breakthrough, the capacities for propane and propene are 1.63 and 1.268 mmol g^{-1}, respectively. Breakthrough curves recorded at 5 bar total pressure (Fig. S12) show an expected decrease in selectivity for propane.

The column breakthrough experiment rules out any significant molecular sieving or kinetic separation in this Zr-fumarate-MOF sample. However, Zr-fumarate-MOF was recently used to create a mixed-matrix membrane which was shown to have an improved selectivity for propylene (approximately 10), above the theoretical upper bound of a pure polymer membrane[45]. The authors attribute the result to a conformation-controlled sieving effect which allows for faster diffusion of propylene through the crystal. The marked difference between the adsorption behaviour of the two samples can be explained by the additional porosity introduced by the presence of missing cluster defects. This would increase the diffusion rates of both probes inside the crystal and allow for communication between different pores through the resulting channels. This pore network can explain the relatively fast kinetics of adsorption observed with both propane and propylene in our sample, in contrast to what is likely to be a more "perfect" material.

When comparing the performance of defective Zr-fumarate-MOF with other adsorbents, propane selectivity is rarely observed. Several studies also highlight a slight thermodynamic preference for paraffins over olefins in adsorbents such as AlMePO-α[19] IRMOF-8[68] and MIL-53(Al)-FA[69] In these cases, as with Zr-fumarate-MOF the preference for propane is attributed to stronger non-specific interactions with the structure. However, Zr-fumarate-MOF is, to the best of our knowledge, the first adsorbent which can be switched between kinetic selectivity for propylene and thermodynamic selectivity for propane through defect engineering.

3. Conclusions

In this study, the adsorption of saturated and monounsaturated C3 hydrocarbons on a sample of Zr-fumarate-MOF synthesised with a large excess of formic acid modulator was studied through a combined experimental and simulation methodology. Anomalous results highlighted through microcalorimetry screening and experimental isotherms were explained on the basis of material defects. Two types of defect — missing linker and missing cluster — in various concentrations and conformations in the material structure have been simulated. It was found that missing linker defects have little effect on the equilibrium adsorption behaviour of C3 hydrocarbons and that the experimental isotherms can best be described by a model where $1/8^{\text{th}}$ of the total zirconium clusters are missing.

We have also shown that the phonon vibrational modes can favour adsorbate diffusion in the pristine material. Logically, they must also have an influence on adsorption in the defective structure, especially, when the pore apertures is comparable with the kinetic diameter of the adsorbate. In such case, dynamic deformations of low frequency phonons will substantially facilitate adsorption.

Surprisingly, mixture co-adsorption GCMC simulations and IAST predictions on the material suggest a preference for propane over propylene adsorption, contrary to what can be expected on a pristine structure[45]. Column breakthrough experiments corroborate this effect, with resulting breakthrough curves suggesting relatively fast kinetics for both probes. Therefore, it is logical to postulate that the presence of structural defects can drastically affect the separation of the C3 mixture, and may ultimately be employed as an avenue for tuning separation performance.

Overall, this work furthers the understanding of the role of defects in Zr-fumarate-MOF (or MOF-801). In this case, the introduction of defects led to an unexpected change in selectivity from propylene to propane. Although the separation factor is too low for practical applications, this behaviour opens the door to the possibility of materials which allow for the recovery of propylene in the raffinate stream, a property highly desirable in a PSA/TSA separation processes. Our work shows that the selectivity of MOFs in separation processes can in principle be controlled using their defect chemistry, posing the challenge to further develop the methods of defect engineering.

4. Materials and methods

Details pertaining to the synthesis of the Zr-fumarate-MOF, its characterisation and the computational modelling can be found in the Supporting Information.

Acknowledgements

PI, PLL, JM and RA have received funding from the European Union's Horizon 2020 research and innovation programme under the Marie Sklodowska-Curie grant agreement No 641887 (project acronym: DEFNET). FF, JR and BK are supported by the Polish National Science Centre (NCN, grant no. 2015/17/B/ST8/00099). JS acknowledges the financial support from the Research Grants Council of Hong Kong (CityU 21301817). This research was supported in part by PL-Grid Infrastructure. FF thanks Dr. Halina Maniak for insightful discussions on coordinational chemistry.

Author contributions

PI and FF elaborated the manuscript draft, with major contributions from JM. AM synthesised all material used. PI performed characterisation through adsorption, microcalorimetry, SEM and TGA. JM measured and analysed ^{1}H NMR and PXRD data. Column breakthrough experiments were carried

out by JS. FF and JR carried out all computational calculations. All authors contributed for manuscript review and editing. Work was supervised by RA, PB, BK and PLL.

References

1. "North America Propylene Supply Study." Tech. rep., IHS Markit, 2018
2. Eldridge, R.B. "Olefin/paraffin separation technology: A review." *Industrial & Engineering Chemistry Research*, 1993. **32**(10):2208–2212. doi:10.1021/ie00022a002
3. Jarvelin, H. and Fair, J.R. "Adsorptive separation of propylene-propane mixtures." *Industrial & Engineering Chemistry Research*, 1993. **32**(10):2201–2207. doi:10.1021/ie00022a001
4. "Hybrid Separations/Distillation Technology: Research Opportunities for Energy and Emissions Reduction." Tech. rep., USA Department of Energy, 2005
5. Shimazu, A.; Miyazaki, T.; Maeda, M.; and Ikeda, K. "Relationships between the chemical structures and the solubility, diffusivity, and permselectivity of propylene and propane in 6FDA-based polyimides." *Journal of Polymer Science Part B: Polymer Physics*, 2000. **38**(19):2525–2536. doi:10.1002/1099-0488(20001001)38:19<2525::AID-POLB40>3.0.CO;2-2
6. Ilinitch, O.; Semin, G.; Chertova, M.; and Zamaraev, K. "Novel polymeric membranes for separation of hydrocarbons." *Journal of Membrane Science*, 1992. **66**(1):1–8. doi:10.1016/0376-7388(92)80085-X
7. Tanaka, K.; Taguchi, A.; Hao, J.; Kita, H.; and Okamoto, K. "Permeation and separation properties of polyimide membranes to olefins and paraffins." *Journal of Membrane Science*, 1996. **121**(2):197–207. doi:10.1016/S0376-7388(96)00182-2
8. Glanz, P. and Findenegg, G.H. "Adsorption of Gas Mixtures of Propene and Propane on Graphitized Carbon Black I. Experimental Method and Results." *Adsorption Science & Technology*, 1984. **1**(1):41–50. doi:10.1177/026361748400100103
9. Liu, J.; Liu, Y.; Kayrak Talay, D.; Calverley, E.; Brayden, M.; and Martinez, M. "A new carbon molecular sieve for propylene/propane separations." *Carbon*, 2015. **85**:201–211. doi:10.1016/j.carbon.2014.12.089
10. Glanz, P.; Körner, B.; and Findenegg, G.H. "Adsorption of Propene and Propane on Graphitized Carbon. II. Analysis of Single Gas and Mixed Gas Isotherms." *Adsorption Science & Technology*, 1984. **1**(3):183–193. doi:10.1177/026361748400100301
11. Shu, C.; Kulvaranon, S.; Findley, M.; and Liapis, A. "Experimental and computational studies on propane-propylene separation by adsorption and variable-temperature stepwise desorption." *Separations Technology*, 1990. **1**(1):18–28. doi:10.1016/0956-9618(90)80003-X
12. Schoellner, R. and Mueller, U. "Influence of Mono- and Bivalent Cations in 4A-Zeolites on the Adsorptive Separation of Ethene and Propene from Crack-Gases." *Adsorption Science & Technology*, 1986. **3**(3):167–171. doi:10.1177/026361748600300306
13. Combariza, A.F.; Sastre, G.; and Corma, A. "Propane/Propylene Diffusion in Zeolites: Framework Dynamics." *The Journal of Physical Chemistry C*, 2009. **113**(26):11246–11253. doi:10.1021/jp903245j
14. Grande, C.A.; Gigola, C.; and Rodrigues, A.E. "Adsorption of Propane and Propylene in Pellets and Crystals of 5A Zeolite." *Industrial & Engineering Chemistry Research*, 2002. **41**(1):85–92. doi:10.1021/ie010494o
15. Selzer, C.; Werner, A.; and Kaskel, S. "Selective Adsorption of Propene over Propane on Hierarchical Zeolite ZSM-58." *Industrial & Engineering Chemistry Research*, 2018. **57**(19):6609–6617. doi:10.1021/acs.iecr.8b00377
16. Khalighi, M.; Chen, Y.F.; Farooq, S.; Karimi, I.A.; and Jiang, J.W. "Propylene/Propane Separation Using SiCHA." *Industrial & Engineering Chemistry Research*, 2013. **52**(10):3877–3892. doi:10.1021/ie3026955
17. Grande, C.A.; Araujo, J.D.P.; Cavenati, S.; Firpo, N.; Basaldella, E.; and Rodrigues, A.E. "New π-Complexation Adsorbents for Propane-Propylene Separation." *Langmuir*, 2004. **20**(13):5291–5297. doi:10.1021/la036400s
18. Safarik, D.J. and Eldridge, R.B. "Olefin/Paraffin Separations by Reactive Absorption: A Review." *Industrial & Engineering Chemistry Research*, 1998. **37**(7):2571–2581. doi:10.1021/ie970897h
19. Kroon, M.C. and Vega, L.F. "Selective Paraffin Removal from Ethane/Ethylene Mixtures by Adsorption into Aluminum Methylphosphonate-α: A Molecular Simulation Study." *Langmuir*, 2009. **25**(4):2148–2152. doi:10.1021/la803042z
20. Koros, W.J. and Mahajan, R. "Pushing the limits on possibilities for large scale gas separation: Which strategies?" *Journal of Membrane Science*, 2000. **175**(2):181–196. doi:10.1016/S0376-7388(00)00418-X
21. Ruthven, D.M. *Principles of Adsorption and Adsorption Processes*. Wiley, New York, 1984. ISBN 978-0-471-86606-0
22. Zhu, W.; Kapteijn, F.; Moulijn, J.A.; den Exter, M.C.; and Jansen, J.C. "Shape Selectivity in Adsorption on the All-Silica DD3R." *Langmuir*, 2000. **16**(7):3322–3329. doi:10.1021/la9914007
23. Olson, D.H.; Camblor, M.A.; Villaescusa, L.A.; and Kuehl, G.H. "Light hydrocarbon sorption properties of pure silica Si-CHA and ITQ-3 and high silica ZSM-58." *Microporous and Mesoporous Materials*, 2004. **67**(1):27–33. doi:10.1016/j.micromeso.2003.09.025
24. Gascon, J.; Blom, W.; van Miltenburg, A.; Ferreira, A.; Berger, R.; and Kapteijn, F. "Accelerated synthesis of all-silica DD3R and its performance in the separation of propylene/propane mixtures." *Microporous and Mesoporous Materials*, 2008. **115**(3):585–593. doi:10.1016/j.micromeso.2008.02.038
25. Rubeš, M.; Wiersum, A.D.; Llewellyn, P.L.; Grajciar, L.; Bludský, O.; Nachtigall, P.; Rubes, M.; Wiersum, A.D.; Llewellyn, P.L.; Grajciar, L.; Bludský, O.; and Nachtigall, P. "Adsorption of propane and propylene on CuBTC metal-organic framework: Combined theoretical and experimental investigation." *Journal of Physical Chemistry C*, 2013. **117**(21):11159–11167. doi:10.1021/jp401600v
26. Plaza, M.; Ribeiro, A.; Ferreira, A.; Santos, J.; Lee, U.H.; Chang, J.S.; Loureiro, J.; and Rodrigues, A. "Propylene/propane separation by vacuum swing adsorption using Cu-BTC spheres." *Separation and Purification Technology*, 2012. **90**:109–119. doi:10.1016/j.seppur.2012.02.023
27. Yoon, J.W.; Seo, Y.K.; Hwang, Y.K.; Chang, J.S.; Leclerc, H.; Wuttke, S.; Bazin, P.; Vimont, A.; Daturi, M.; Bloch, E.; Llewellyn, P.L.; Serre, C.; Horcajada, P.; Grenèche, J.M.; Rodrigues, A.E.; and Férey, G. "Controlled Reducibility of a Metal-Organic Framework with Coordinatively Unsaturated Sites for Preferential Gas Sorption." *Angewandte Chemie International Edition*, 2010. **49**(34):5949–5952. doi:10.1002/anie.201001230
28. Autie-Castro, G.; Autie, M.; Reguera, E.; Moreno-Tost, R.; Rodríguez-Castellón, E.; Jiménez-López, A.; and Santamaría-González, J. "Adsorption and separation of propane and propylene by porous hexacyanometallates." *Applied Surface Science*, 2011. **257**(7):2461–2466. doi:10.1016/j.apsusc.2010.10.003
29. Lee, C.Y.; Bae, Y.S.; Jeong, N.C.; Farha, O.K.; Sarjeant, A.A.; Stern, C.L.; Nickias, P.; Snurr, R.Q.; Hupp, J.T.; and Nguyen, S.T. "Kinetic Separation of Propene and Propane in Metal-Organic Frameworks: Controlling Diffusion Rates in Plate-Shaped Crystals via Tuning of Pore Apertures and Crystallite Aspect Ratios." *Journal of the American Chemical Society*, 2011. **133**(14):5228–5231. doi:10.1021/ja200553m
30. Assen, A.H.; Belmabkhout, Y.; Adil, K.; Bhatt, P.M.; Xue, D.X.; Jiang, H.; and Eddaoudi, M. "Ultra-Tuning of the Rare-Earth fcu-MOF Aperture Size for Selective Molecular Exclusion of Branched Paraffins." *Angewandte Chemie International Edition*, 2015. **54**(48):14353–14358. doi:10.1002/anie.201506345
31. Pan, Y.; Li, T.; Lestari, G.; and Lai, Z. "Effective separation of propylene/propane binary mixtures by ZIF-8 membranes." *Journal of Membrane Science*, 2012. **390-391**:93–98. doi:10.1016/j.memsci.2011.11.024
32. Li, K.; Olson, D.H.; Seidel, J.; Emge, T.J.; Gong, H.; Zeng, H.; and Li, J. "Zeolitic Imidazolate Frameworks for Kinetic Separation of Propane and Propene." *Journal of the American Chemical Society*, 2009. **131**(30):10368–10369. doi:10.1021/ja9039983
33. Gücüyener, C.; van den Bergh, J.; Gascon, J.; and Kapteijn, F. "Ethane/Ethene Separation Turned on Its Head: Selective Ethane Adsorption on the Metal-Organic Framework ZIF-7 through a Gate-Opening Mechanism." *Journal of the American Chemical Society*, 2010. **132**(50):17704–17706. doi:10.1021/ja1089765
34. van den Bergh, J.; Gücüyener, C.; Pidko, E.A.; Hensen, E.J.M.; Gascon, J.; and Kapteijn, F. "Understanding the Anomalous Alkane Selectivity of ZIF-7 in the Separation of Light Alkane/Alkene Mixtures." *Chemistry - A European Journal*, 2011. **17**(32):8832–8840. doi:10.1002/chem.201100958
35. Fairen-Jimenez, D.; Moggach, S.A.; Wharmby, M.T.; Wright, P.A.; Parsons, S.; and Düren, T. "Opening the Gate: Framework Flexibility in ZIF-8 Explored by Experiments and Simulations." *Journal of the American Chemical Society*, 2011. **133**(23):8900–8902. doi:10.1021/ja202154j
36. Wißmann, G.; Schaate, A.; Lilienthal, S.; Bremer, I.; Schneider, A.M.; and Behrens, P. "Modulated synthesis of Zr-fumarate MOF." *Microporous and Mesoporous Materials*, 2012. **152**:64–70. doi:10.1016/j.micromeso.2011.12.010
37. Furukawa, H.; Gándara, F.; Zhang, Y.B.; Jiang, J.; Queen, W.L.; Hudson, M.R.; and Yaghi, O.M. "Water Adsorption in Porous Metal–Organic Frameworks and Related Materials." *Journal of the American Chemical Society*, 2014. **136**(11):4369–4381. doi:10.1021/ja500330a
38. Ren, J.; Musyoka, N.M.; Langmi, H.W.; North, B.C.; Mathe, M.; Pang, W.; Wang, M.; and Walker, J. "In-situ IR monitoring of the formation of Zr-fumarate MOF." *Applied Surface Science*, 2017. **404**:263–267. doi:10.1016/j.apsusc.2017.01.271
39. Zahn, G.; Schulze, H.A.; Lippke, J.; König, S.; Sazama, U.; Fröba, M.; and Behrens, P. "A water-born Zr-based porous coordination polymer: Modulated synthesis of Zr-fumarate MOF." *Microporous and Mesoporous Materials*, 2015. **203**:186–194. doi:10.1016/j.micromeso.2014.10.034
40. Reinsch, H.; Waitschat, S.; Chavan, S.M.; Lillerud, K.P.; and Stock, N. "A Facile "Green" Route for Scalable Batch Production and Continuous Synthesis of Zirconium MOFs: A Facile "Green" Route for Scalable Batch Production and Continuous Synthesis of Zirconium MOFs." *European Journal of Inorganic Chemistry*, 2016. **2016**(27):4490–4498. doi:10.1002/ejic.201600295
41. Bueken, B.; Van Velthoven, N.; Willhammar, T.; Stassin, T.; Stassen, I.; Keen, D.A.; Baron, G.V.; Denayer, J.F.M.; Ameloot, R.; Bals, S.; De Vos, D.; and Bennett, T.D. "Gel-based morphological design of zirconium metal–organic frameworks." *Chemical Science*, 2017. **8**(5):3939–3948. doi:10.1039/C6SC05602D
42. Bae, Y.J.; Cho, E.S.; Qiu, F.; Sun, D.T.; Williams, T.E.; Urban, J.J.; and Queen, W.L. "Transparent Metal–Organic Framework/Polymer Mixed Matrix Membranes as Water Vapor Barriers." *ACS Applied Materials & Interfaces*, 2016. **8**(16):10098–10103. doi:10.1021/acsami.6b01299
43. Kim, H.; Yang, S.; Rao, S.R.; Narayanan, S.; Kapustin, E.A.; Furukawa, H.; Umans, A.S.; Yaghi, O.M.; and Wang, E.N. "Water harvesting from air with metal-organic frameworks powered by natural sunlight." *Science*, 2017. **356**(6336):430–434. doi:10.1126/science.aam8743
44. Choi, J.; Lin, L.C.; and Grossman, J.C. "Role of Structural Defects in the Water Adsorption Properties of MOF-801." *The Journal of Physical Chemistry C*, 2018. **122**(10):5545–5552. doi:10.1021/acs.jpcc.8b00014
45. Liu, Y.; Chen, Z.; Liu, G.; Belmabkhout, Y.; Adil, K.; Eddaoudi, M.; and Koros, W. "Conformation-Controlled Molecular Sieving Effects for Membrane-Based Propylene/Propane Separation." *Advanced Materials*, 2019. p. 1807513. doi:10.1002/adma.201807513
46. Dubbeldam, D.; Calero, S.; and Vlugt, T.J. "iRASPA: GPU-accelerated visualization software for materials scientists." *Molecular Simulation*, 2018. **44**(8):653–676. doi:10.1080/08927022.2018.1426855
47. Zahn, G.; Zerner, P.; Lippke, J.; Kempf, F.L.; Lilienthal, S.; Schröder, C.A.; Schneider, A.M.; and Behrens, P. "Insight into the mechanism of modulated syntheses: *In Situ* synchrotron diffraction studies on the formation of Zr-fumarate MOF." *CrystEngComm*, 2014. **16**(39):9198–9207. doi:10.1039/C4CE01095G
48. Liu, B.; Smit, B.; Rey, F.; Valencia, S.; and Calero, S. "A New United Atom Force Field for Adsorption of Alkenes in Zeolites." *The Journal of Physical Chemistry C*, 2008. **112**(7):2492–2498. doi:10.1021/jp075809d
49. Luna-Triguero, A.; Vicent-Luna, J.M.; Becker, T.M.; Vlugt, T.J.H.; Dubbeldam, D.; Gómez-Álvarez, P.; and Calero, S. "Effective Model for Olefin/Paraffin Separation using (Co, Fe, Mn, Ni)-MOF-74." *ChemistrySelect*, 2017. **2**(2):665–672. doi:10.1002/slct.201601095
50. Luna-Triguero, A.; Vicent-Luna, J.M.; Gómez-Álvarez, P.; and Calero, S. "Olefin/Paraffin Separation in Open Metal Site Cu-BTC Metal–Organic Framework." *The Journal of Physical Chemistry C*, 2017. **121**(5):3126–3132. doi:10.1021/acs.jpcc.6b11808

51. Luna-Triguero, A.; Vicent-Luna, J.M.; Dubbeldam, D.; Gómez-Álvarez, P.; and Calero, S. "Understanding and Exploiting Window Effects for Adsorption and Separations of Hydrocarbons." *The Journal of Physical Chemistry C*, 2015. **119**(33):19236–19243. doi:10.1021/acs.jpcc.5b05597
52. Min, J.G.; Luna-Triguero, A.; Byun, Y.; Balestra, S.R.G.; Vicent-Luna, J.M.; Calero, S.; Hong, S.B.; and Camblor, M.A. "Stepped Propane Adsorption in Pure-Silica ITW Zeolite." *Langmuir*, 2018. **34**(16):4774–4779. doi:10.1021/acs.langmuir.8b00628
53. Ryder, M.R.; Civalleri, B.; Bennett, T.D.; Henke, S.; Rudić, S.; Cinque, G.; Fernandez-Alonso, F.; and Tan, J.C. "Identifying the Role of Terahertz Vibrations in Metal-Organic Frameworks: From Gate-Opening Phenomenon to Shear-Driven Structural Destabilization." *Physical Review Letters*, 2014. **113**(21):215502. doi:10.1103/PhysRevLett.113.215502
54. Rogacka, J.; Formalik, F.; Triguero, A.L.; Firlej, L.; Kuchta, B.; and Calero, S. "Intermediate states approach for adsorption studies in flexible metal–organic frameworks." *Physical Chemistry Chemical Physics*, 2019. **21**(6):3294–3303. doi:10.1039/C8CP06817H
55. Sarkisov, L. and Harrison, A. "Computational structure characterisation tools in application to ordered and disordered porous materials." *Molecular Simulation*, 2011. **37**(15):1248–1257. doi:10.1080/08927022.2011.592832
56. Vermoortele, F.; Bueken, B.; Le Bars, G.; Van de Voorde, B.; Vandichel, M.; Houthoofd, K.; Vimont, A.; Daturi, M.; Waroquier, M.; Van Speybroeck, V.; Kirschhock, C.; and De Vos, D.E. "Synthesis Modulation as a Tool To Increase the Catalytic Activity of Metal–Organic Frameworks: The Unique Case of UiO-66(Zr)." *Journal of the American Chemical Society*, 2013. **135**(31):11465–11468. doi:10.1021/ja405078u
57. Ghosh, P.; Colón, Y.J.; and Snurr, R.Q. "Water adsorption in UiO-66: The importance of defects." *Chem Commun*, 2014. **50**(77):11329–11331. doi:10.1039/C4CC04945D
58. Gutov, O.V.; Hevia, M.G.; Escudero-Adán, E.C.; and Shafir, A. "Metal–Organic Framework (MOF) Defects under Control: Insights into the Missing Linker Sites and Their Implication in the Reactivity of Zirconium-Based Frameworks." *Inorganic Chemistry*, 2015. **54**(17):8396–8400. doi:10.1021/acs.inorgchem.5b01053
59. Trickett, C.A.; Gagnon, K.J.; Lee, S.; Gándara, F.; Bürgi, H.B.; and Yaghi, O.M. "Definitive Molecular Level Characterization of Defects in UiO-66 Crystals." *Angewandte Chemie International Edition*, 2015. **54**(38):11162–11167. doi:10.1002/anie.201505461
60. Chen, Z.; Feng, L.; Liu, L.; Bhatt, P.M.; Adil, K.; Emwas, A.H.; Assen, A.H.; Belmabkhout, Y.; Han, Y.; and Eddaoudi, M. "Enhanced Separation of Butane Isomers via Defect Control in a Fumarate/Zirconium-Based Metal Organic Framework." *Langmuir*, 2018. **34**(48):14546–14551. doi:10.1021/acs.langmuir.8b03085
61. Thornton, A.W.; Babarao, R.; Jain, A.; Trousselet, F.; and Coudert, F.X. "Defects in metal–organic frameworks: A compromise between adsorption and stability?" *Dalton Trans*, 2016. **45**(10):4352–4359. doi:10.1039/C5DT04330A
62. Shearer, G.C.; Chavan, S.; Bordiga, S.; Svelle, S.; Olsbye, U.; and Lillerud, K.P. "Defect Engineering: Tuning the Porosity and Composition of the Metal-Organic Framework UiO-66 via Modulated Synthesis." *Chemistry of Materials*, 2016. **28**(11):3749–3761. doi:10.1021/acs.chemmater.6b00602
63. Marreiros, J.; Caratelli, C.; Hajek, J.; Krajnc, A.; Fleury, G.; Bueken, B.; De Vos, D.E.; Mali, G.; Roeffaers, M.B.J.; Van Speybroeck, V.; and Ameloot, R. "Active Role of Methanol in Post-Synthetic Linker Exchange in the Metal–Organic Framework UiO-66." *Chemistry of Materials*, 2019. **31**(4):1359–1369. doi:10.1021/acs.chemmater.8b04734
64. Cliffe, M.J.; Wan, W.; Zou, X.; a Chater, P.; Kleppe, A.K.; Tucker, M.G.; Wilhelm, H.; Funnell, N.P.; Coudert, F.X.; and Goodwin, A.L. "Correlated defect nanoregions in a metal-organic framework." *Nature communications*, 2014. **5**(May):4176. doi:10.1038/ncomms5176
65. Shearer, G.C.; Chavan, S.; Ethiraj, J.; Vitillo, J.G.; Svelle, S.; Olsbye, U.; Lamberti, C.; Bordiga, S.; and Lillerud, K.P. "Tuned to Perfection: Ironing Out the Defects in Metal–Organic Framework UiO-66." *Chemistry of Materials*, 2014. **26**(14):4068–4071. doi:10.1021/cm501859p
66. Taddei, M.; Wakeham, R.J.; Koutsianos, A.; Andreoli, E.; and Barron, A.R. "Post-synthetic ligand exchange in zirconium-based metal-organic frameworks: Beware of the defects!" *Angewandte Chemie International Edition*, 2018. doi:10.1002/anie.201806910
67. Bueken, B.; Reinsch, H.; Reimer, N.; Stassen, I.; Vermoortele, F.; Ameloot, R.; Stock, N.; Kirschhock, C.E.A.; and De Vos, D. "A zirconium squarate metal–organic framework with modulator-dependent molecular sieving properties." *Chem Commun*, 2014. **50**(70):10055–10058. doi:10.1039/C4CC03764B
68. Pires, J.; Pinto, M.L.; and Saini, V.K. "Ethane Selective IRMOF-8 and Its Significance in Ethane–Ethylene Separation by Adsorption." *ACS Applied Materials & Interfaces*, 2014. **6**(15):12093–12099. doi:10.1021/am502686g
69. Peng, J.; Sun, Y.; Wu, Y.; Lv, Z.; and Li, Z. "Selectively Trapping Ethane from Ethylene on Metal–Organic Framework MIL-53(Al)-FA." *Industrial & Engineering Chemistry Research*, 2019. **58**(19):8290–8295. doi:10.1021/acs.iecr.9b00183